Frontiers of Information Technology & Electronic Engineering
www.jzus.zju.edu.cn; engineering.cae.cn; www.springerlink.com
ISSN 2095-9184 (print); ISSN 2095-9230 (online)
E-mail: jzus@zju.edu.cn

De-scattering and edge-enhancement algorithms for underwater image restoration*

Pan-wang PAN[1,2], Fei YUAN[†‡1,2], En CHENG[1,2]

[1]*MOE Key Laboratory of Underwater Acoustic Communication and Marine Information Technology, Xiamen University, Xiamen 361005, China*

[2]*Department of Communication Engineering, Xiamen University, Xiamen 361005, China*

[†]E-mail: yuanfei@xmu.edu.cn

Received Nov. 10, 2017; Revision accepted July 12, 2018; Crosschecked June 11, 2019

Abstract: Image restoration is a critical procedure for underwater images, which suffer from serious color deviation and edge blurring. Restoration can be divided into two stages: de-scattering and edge enhancement. First, we introduce a multi-scale iterative framework for underwater image de-scattering, where a convolutional neural network is used to estimate the transmission map and is followed by an adaptive bilateral filter to refine the estimated results. Since there is no available dataset to train the network, a dataset which includes 2000 underwater images is collected to obtain the synthetic data. Second, a strategy based on white balance is proposed to remove color casts of underwater images. Finally, images are converted to a special transform domain for denoising and enhancing the edge using the non-subsampled contourlet transform. Experimental results show that the proposed method significantly outperforms state-of-the-art methods both qualitatively and quantitatively.

Key words: Image de-scattering; Edge enhancement; Convolutional neural network; Non-subsampled contourlet transform
https://doi.org/10.1631/FITEE.1700744 **CLC number:** TP391.41

1 Introduction

There is much research in underwater imaging in several fields, such as marine resource exploration, environmental protection and monitoring, underwater equipment inspection, and terrain exploration (Wang et al., 2015). Because of the absorption and scattering of light caused by water and suspended particulates, the clarity of an image can be severely reduced. Under the underwater environment, not only is sunlight absorbed, but also colors drop off one by one depending on their wavelengths. Red disappears at a depth of 3 m, and yellow vanishes at 10 m. With the increase of the depth, only blue and green will exist because of the short wavelengths. Therefore, underwater images are dominated mainly by blue and green (Iqbal et al., 2010). As a result, it is difficult to further analyze and study underwater images. The problem can be directly tackled using specialized hardware, which includes polarization and range-gated imaging approaches (Schechner and Karpel, 2006; Tan et al., 2007). However, the above-mentioned methods are inapplicable to ocean engineering applications because of high cost. Recently, many software-based methods have been proposed to improve the clarity of degraded underwater images. They can be divided into two main categories: enhancement algorithms based on image features and restoration algorithms based on degradation models.

Enhancement algorithms do not depend on the reasons of image quality degradation. Pixels are operated in spatial or frequency domains to directly improve the brightness and color characteristics. Histogram equalization (Thakur and Tripathi, 2010) is a typical enhancement method. Although the

‡ Corresponding author

* Project supported by the National Natural Science Foundation of China (Nos. 61571377, 61471308, and 61771412) and the Fundamental Research Funds for the Central Universities, China (No. 20720180068)

ORCID: Fei YUAN, http://orcid.org/0000-0002-8614-8756

overall contrast is improved, it may simultaneously over-enhance the background light. Adaptive histogram equalization (Mao and Jin, 2010) can maintain contour and detailed information, but it may bring about a blocking artifact to underwater images. Homomorphic filtering (Padmavathi et al., 2010) can solve the problem of uneven illumination and enhance detailed information, but it cannot achieve ideal results for complex and changing underwater environments. Underwater images have been transformed into the wavelet domain for de-noising and edge enhancement (Vasamsetti et al., 2017). However, enhancement algorithms do not follow any degradation model and have poor robustness under changing underwater environments.

Algorithms based on degradation models give consideration to the cause of image degradation. Treibitz and Schechner (2009) proposed an algorithm based on an underwater physical degradation model, which estimates the scattered light of the medium with different polarization conditions. It is significantly aided by inter-frame information. In this study, we focus on an image restoration algorithm using a single image. Considering that the underwater image degradation model is similar to an atmospheric scattering model, many researchers use the haze removal algorithm for underwater images. The transmission map was estimated based on the attenuation of the red-green-blue (RGB) channels (Carlevaris-Bianco et al., 2010), but the difference of the attenuation of the RGB channels was ignored. Drews et al. (2013) proposed an underwater dark channel prior (UDCP), where the dark channel was calculated by only blue and green channels. Cai et al. (2016) calculated the transmission map by a deep learning network. Yang et al. (2017) combined the underwater imaging model with a retinex enhancement method, and proposed an underwater restoration algorithm based on L1 regularization. Despite the remarkable progress on underwater image restoration methods, it is still an open problem.

2 De-scattering algorithm

2.1 Underwater imaging model

According to the simplified McGlamery-Jaffe underwater image formation model (Tarel et al., 2012), an imaging model consisting of two parts can be described as

$$I(x)=J^C(x)t(x)+B(x)\big(1-t(x)\big),\ C\in\{\mathrm{r,g,b}\},\quad(1)$$

where $I(x)$ is a degraded image, $J(x)$ the real scene to be recovered, $B(x)$ the global background light, and $t(x)=\exp[-c\lambda d(x)]$ the transmission map with c the light attenuation coefficient, λ the wavelength of light, and $d(x)$ the distance between the scene and camera.

Since red channel attenuation is the most serious, dark channel $J_{\mathrm{dark}}(x)$ can be calculated as

$$J_{\mathrm{dark}}(x)=\min_{y\in\Omega(x)}\Big(\min_{C\in\{\mathrm{g,b}\}}J^C(y)\Big),\quad(2)$$

where $J^C(y)$ is C-color channels of the real scene and $\Omega(x)$ a local patch centered at the x axis with the size of 5×5 pixels. The global background light $B(x)$ is an RGB vector, denoting the intensity of the light at RGB color channels. The brightest pixels of the top 0.1% are selected in the underwater dark channel, and the background light is estimated by the corresponding pixels of the acquired image:

$$B=I\cdot\arg\max\sum_{C\in\{\mathrm{r,g,b}\}}I^C(x),\ x\in P_{0.1\%}.\quad(3)$$

Fig. 1 depicts several results of the estimated background light for underwater images.

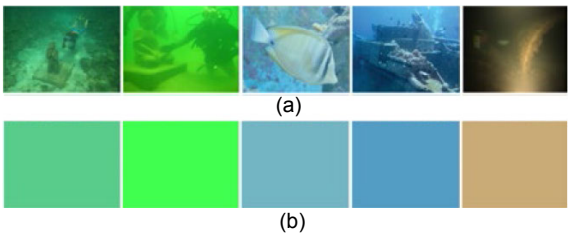

Fig. 1 Results of the estimated global background light: (a) raw underwater images; (b) estimated global background light

On the basis of the transmission map and the background light, a haze-free image can be restored by

$$J(x)=\frac{I(x)-B(x)}{\max\big(t_0,t(x)\big)}+B(x),\quad(4)$$

where t_0 is a constant preventing the value of the denominator from being 0. A typical value of t_0 is 0.1.

To solve the problem that the medium transmission map cannot be accurately calculated because of light absorption, a multi-scale framework inspired by the pyramid decomposition method is proposed. We first decompose underwater images and apply a convolutional neural network (CNN) architecture to estimate the transmission map. We use an adaptive bilateral filter to refine the transmission map, and then apply the white balance technique to remove unrealistic color casts. Fig. 2 depicts the block diagram of the proposed de-scattering algorithm.

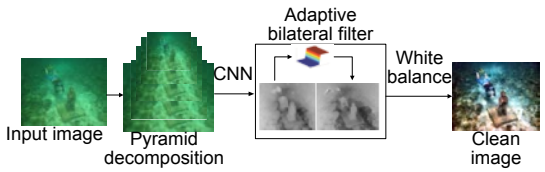

Fig. 2 Flow diagram of the de-scattering algorithm

2.2 Designs of the de-scattering network

2.2.1 Network architecture

The architecture of the proposed de-scattering network is shown in Fig. 3 and Table 1. It contains four convolutional layers with the Maxout (Goodfellow et al., 2013), BReLU (Cai et al., 2016) activation function, and one max pooling layer. In the feature extraction stage, two convolution layers and the Maxout activation function are used to extract features. Since the multi-scale mapping architecture will improve the robustness of feature extraction results (Tang et al., 2014), our de-scattering network extracts the features with three filters of different scales (i.e., 3×3, 5×5, and 7×7 pixels). The main role of the local extremum is down-sampling. Therefore, the output feature maps can remove unnecessary redundant information and suppress the noise of the estimated transmittance map. The value of the transmittance map changes between 0 and 1; therefore, it must apply BReLU to normalize the network output to this range.

Table 1 An architecture of the de-scattering network

Convolutional layer	Type	Input size	Number (n)	Filter	Padding
Feature extraction	Conv	3×16×16	16	5×5	0
	Maxout	16×12×12	4		0
	Conv	3×16×16	16	5×5	0
	Maxout	16×12×12	4		0
Multi-scale mapping	Conv	4×12×12	16	3×3	1
			16	5×5	2
			16	7×7	3
Local extremum	Maxpool	48×12×12	–	7×7	0
Non-linear regression	Conv	48×6×6	1	6×6	0
	BReLU	1×1	1	–	0

2.2.2 Loss function

Denote the input hazy image and real transmission map as X and Y, respectively. The goal of this study is to directly train a deep CNN architecture $h(X)$ on multiple images to minimize the loss function, expressed as

$$L=\frac{1}{N}\sum_{i=1}^{N}\left\|h(X_i)-Y_i\right\|^2, \tag{5}$$

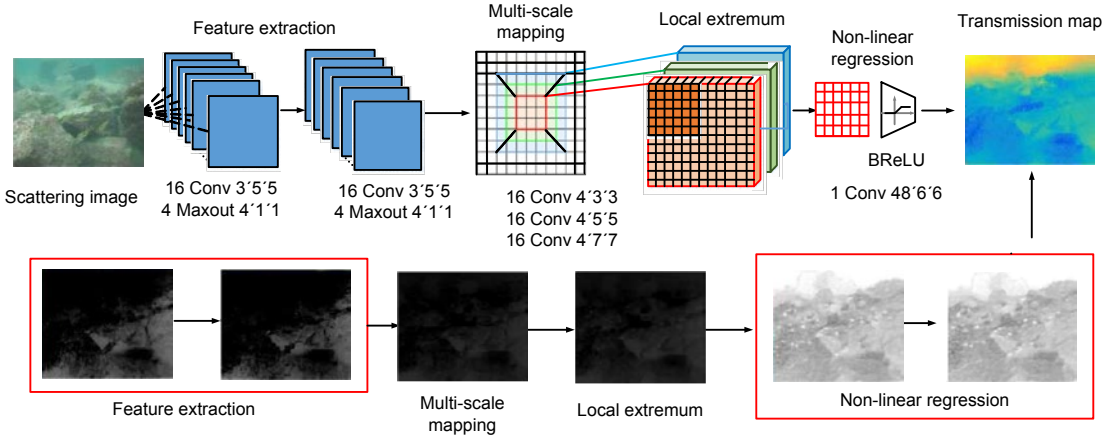

Fig. 3 Schematic of the de-scattering network

where the mean squared error (MSE) is used to measure the difference between the output of the CNN and the real transmission map.

2.2.3 Training

Since it is difficult to collect a large number of clean and hazed image pairs, we synthesize hazed images in Fig. 4 via Eq. (1) to train this network. We collect a dataset of 2000 clean underwater images in Fig. 5, which records with a high frame-rate camera to synthesize hazy images. Each clean image is used to generate five hazy images with different background light and transmission maps.

A stochastic gradient descent (SGD) with a weight decay of 10^{-10}, a momentum of 0.9, and a mini-batch size of 50 are used to minimize loss function (5). After training, the network can be used to output the medium transmission map of an input hazy image.

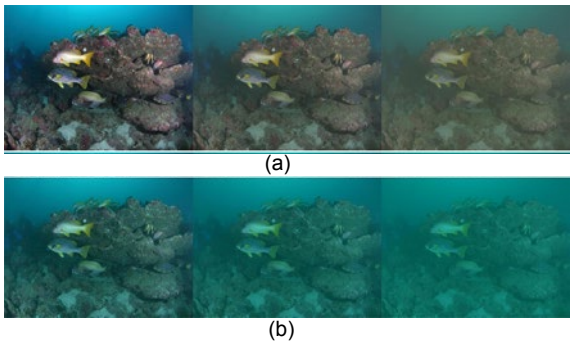

Fig. 4 Underwater color images (a) and synthesized images (b)

2.2.4 Results and refinements

To suppress the blocking artifacts of the patch-based medium transmission map, an adaptive bilateral filter is applied to refine the transmission map. A bilateral filter is given by (Tomasi and Manduchi, 1998)

$$I_{\mathrm{BF}}(p)=\frac{1}{W_p}\sum_{q\in\Omega(p)}G_{\mathrm{s}}(\|p-q\|)G_{\mathrm{r}}(\|I(p)-I(q)\|)I(q), \tag{6}$$

where $\Omega(p)$ is a patch centered at p, s the spatial domain, and r the range domain. W_p is a normalization factor, expressed as

$$W_p=\sum_{q\in\Omega(p)}G_{\mathrm{s}}(\|p-q\|)G_{\mathrm{r}}(\|I(p)-I(q)\|), \tag{7}$$

where G_{s} and G_{r} are Gaussian functions, expressed as

$$G_{\mathrm{s}}(\|p-q\|)=\exp\left(-\frac{\|p-q\|^2}{2\sigma_{\mathrm{s}}^2}\right), \tag{8}$$

$$G_{\mathrm{r}}(\|I(p)-I(q)\|)=\exp\left(-\frac{\|I(p)-I(q)\|^2}{2\sigma_{\mathrm{r}}^2}\right). \tag{9}$$

The weight coefficient of the bilateral filter is determined by the spatial influence factor and the brightness influence factor. The method of adaptive

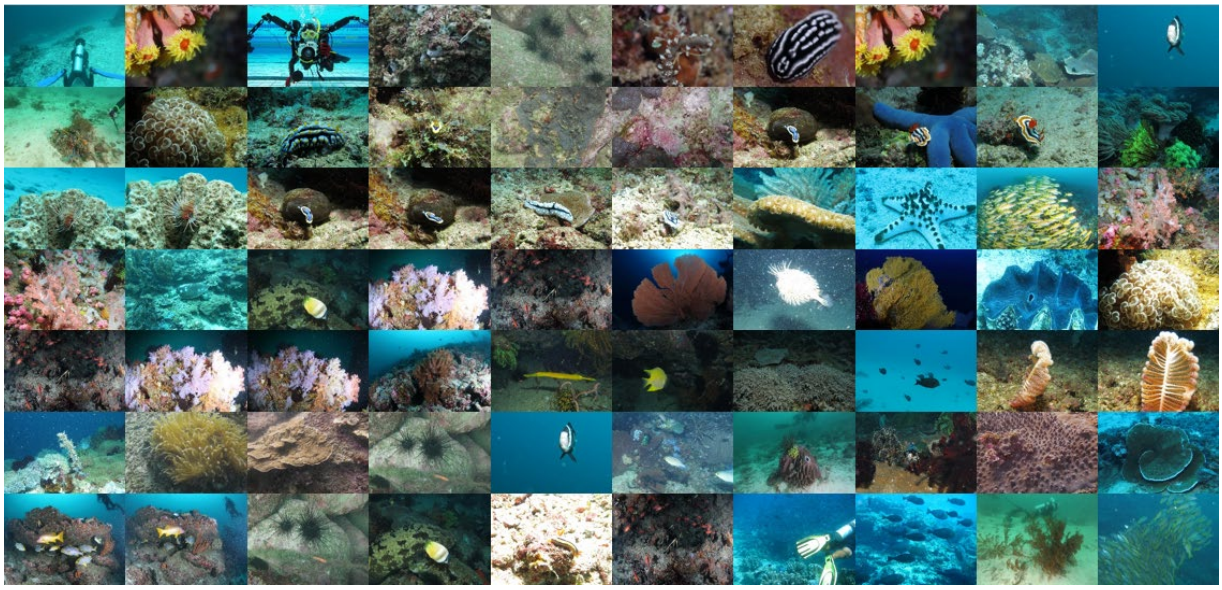

Fig. 5 Examples of haze-free training underwater images recorded by a remotely operated vehicle

bilateral filter is proposed to obtain σ_r by calculating σ_{blk} (the variance of each image patch). Assume the maximum and minimum values for σ_r exist. Then σ_r can be expressed as

$$\sigma_r = \max(\sigma_{r,\min}, \min(\sigma_{r,\max}, k\sigma_{blk})), \quad (10)$$

where k is a positive number, and $\sigma_{r,\max}$ and $\sigma_{r,\min}$ are upper and lower bounds, respectively. Results of transmission maps refined by the adaptive bilateral filter are illustrated in Fig. 6.

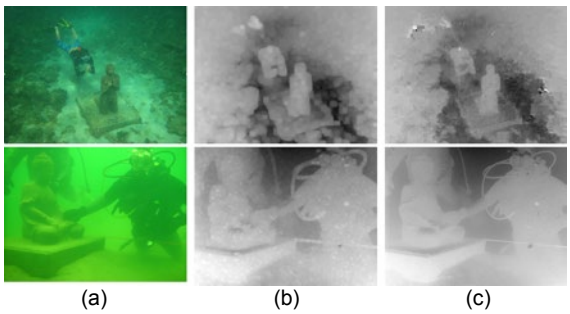

Fig. 6 Original images (a), estimated transmission maps (b), and refined transmission maps (c)

It is clear that the refined transmission maps can suppress the block artifacts to capture the outline of the underwater images.

2.3 White balance

One common problem being noticed during the tests of color correction methods is that underwater images whose appearances are overall blue or green will have a reddish appearance after using the white balance technique. Therefore, it is necessary to find a robust color correction method for underwater images. White balance is a process to remove unrealistic color casts, so that objects which appear white are rendered white in the image.

The Shades-of-Grey (Finlayson and Trezzi, 2004) obtains the illumination of the scene using the Minkowski p-norm. The Shades-of-Grey assumes that the p power of the images' average is gray, so that it obeys

$$Y_{p,i} = \left(\int_w E(\lambda) S_i(\lambda) Y(\lambda) \mathrm{d}\lambda \right)^p = Y_i^p, \quad (11)$$

where λ is the wavelength of the visible light, $E(\lambda)$ the light source, $S_i(\lambda)$ the Lambert surface, and $Y(\lambda)$ the sensor's sensitive function of different wavelengths. Since we assume that the expectation of p-norm of $S(\lambda)$ is a constant, $E_p[S(\lambda)]$ is calculated as

$$E_p[S(\lambda)] = \left(\frac{1}{N} \sum_{i=1}^{N} (S_i(\lambda))^p \right)^{1/p} = \kappa_p, \quad (12)$$

where $E(\cdot)$ denotes the expectation of the corresponding variate. Substituting Eq. (11) into Eq. (12), we can obtain

$$\begin{aligned} E_p[(Y_p)] &= \left(\int_w E_p(\lambda) \sum_{i=1}^{N} \frac{1}{N} (S_i(\lambda))^p Y(\lambda) \mathrm{d}\lambda \right)^{1/p} \\ &= \kappa_p Y_E. \end{aligned} \quad (13)$$

Eq. (13) indicates that the expectation of the p-norm of pixels is a constant multiplied by the ambient light Y_E. In our test results, white balance can remove the color cast most effectively when p is set to six.

Robust auto white balance (AWB) is chosen to correct the phenomenon of severe underwater color shift. The method searches for gray pixels in underwater images and then compares the deviations of these gray points in the YUV color space. According to the comparison of gray-scale deviations, it corrects color deviations through an iterative procedure. Fig. 7 shows the color correction results of an example. The hue histogram results show that the color correction algorithm can eliminate color deviations.

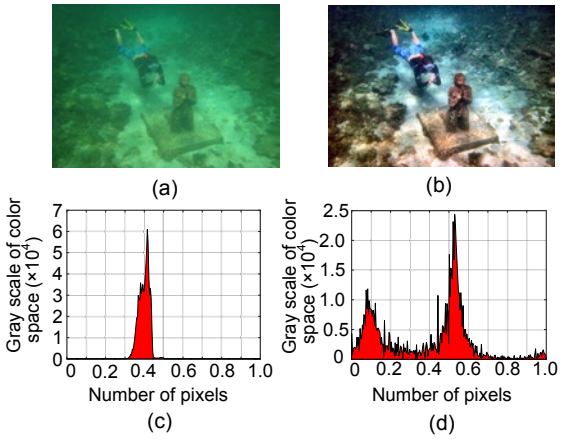

Fig. 7 Original image (a), color corrected image (b), hue histogram of the original image (c), and hue histogram of the color corrected image (d)

3 Edge-enhancement algorithm

3.1 Non-subsampled contourlet transform

Underwater images need to be transformed into a specific domain to remove the noise added in the images and to effectively enhance image edges. Traditional two-dimensional (2D) discrete wavelet transformation (DWT) captures only information of limited directions. Therefore, DWT is generally inadequate for representing geometric structures with a wide range of directionality. Non-subsampled contourlet transform (NSCT) is committed to a new optimal representation of high-dimensional functions. NSCT proposed by Li et al. (2014) consists of two types of filters: non-subsampled pyramid (NSP) and non-subsampled directional filter banks (NSDFB). The NSP is a dual-channel non-sampled filter used for decomposing underwater images. The structure of the NSCT is shown in Fig. 8.

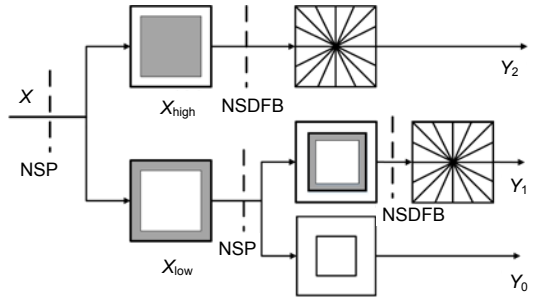

Fig. 8 Diagram of non-subsampled contourlet transform (NSCT)
NSP: non-subsampled pyramid; NSDFB: non-subsampled directional filter banks

Each decomposition output of the next level follows an NSDFB, and the sampling matrix D is set to [2, 0; 0, 2].

Algorithm 1 depicts the process of the NSCT.

Algorithm 1 Non-subsampled contourlet transform

Input: an input image X
Output: a cell vector of matrices and directional subbands Y

Initialize n, $j \leftarrow n+1$
Initialize Y by applying a filter to the first level of X
for i=1 to n do
  Obtain X_{low} and X_{high} via NSP decomposition
  if j>1 then
    Obtain X_{high} by performing NSDFB decomposition at level $j-1$
    $Y_j \leftarrow X_{\text{high}}$
  else
    $Y_j \leftarrow X^{\text{high}}$
  end if
  $j \leftarrow j-1$
  $X \leftarrow X_{\text{low}}$
end for

3.2 Denoising and edge enhancement

We need to not only enhance the edges in underwater images but also suppress noise. Three hard thresholds are used to remove noise while keeping the advantage of edge enhancement. The edge-enhancement algorithm is given by

$$y(x,T)=\begin{cases}0, & x<T_1,\\ \dfrac{x-T_1}{T_1}\left(\dfrac{T_3}{T_2}\right)^{\alpha}+\dfrac{T_2-x}{T_1}, & T_1\le x<T_2,\\ \left(\dfrac{T_3}{x}\right)^{\alpha}, & T_2\le x<T_3,\\ 1, & x\ge T_3,\end{cases} \tag{14}$$

where $T=\{T_1, T_2, T_3\}$ denotes the enhancement threshold and $T_1<T_2<T_3$, and the exponent α denotes the degree of non-linearity. An edge-enhanced underwater image is shown in Fig. 9.

(a) (b)

Fig. 9 An original image (a) and edge-enhanced image (b)

4 Experiments

To demonstrate the contributions of our image enhancement method, we present subjective and objective performance results and compare them with those of several state-of-the-art methods for improving the visibility of images. The entire experiment was tested on Matlab 2015b with a central processing unit (CPU) Intel i7 7700k, 4.2 GHz.

4.1 Subjective performance comparison

As shown in Fig. 10, the proposed method significantly improves the visibility of the actual scattering images and has a best subjective performance compared with two single-image haze removal algorithms.

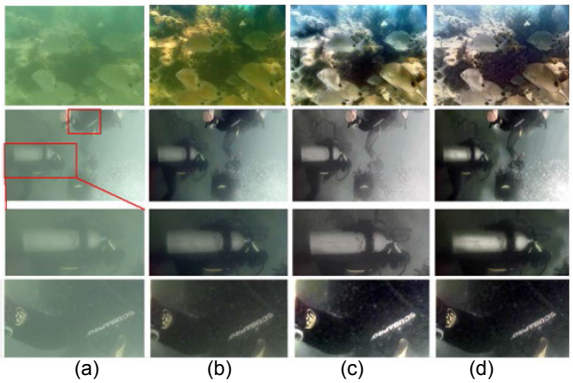

Fig. 10 Original images (a), images restored by He et al. (2011)'s method (b), images restored by Ancuti et al. (2012)'s method (c), and images restored by the proposed method (d)

We can conclude that the proposed method maintains natural appearance and restores information of underwater images (e.g., texture, text, and color). This is because the proposed method is based on a fusion framework and an edge-preserving smoothing operator (adaptive bilateral filtering). He et al. (2011)'s method does not obtain the expected results in raw underwater images because it ignores the selective attenuation of color and has limited effect on transmission map estimation. Ancuti et al., (2012)'s method effectively improves the contrast and eliminates the color deviation of raw underwater images. However, some areas presented in the output are over-enhanced because this method does not rely on prior knowledge of the underwater conditions.

The proposed method is capable of enhancing turbulence blur images owing to the edge enhancement stage. Fig. 11 shows the edge enhancement results of two turbulence blur images, and compares them with a blind deblurring algorithm (Pan et al., 2016). It shows that the edge region and visibility of underwater images are enhanced by the proposed method and that it obtains clearer and sharper edges than Pan et al. (2016)'s algorithm.

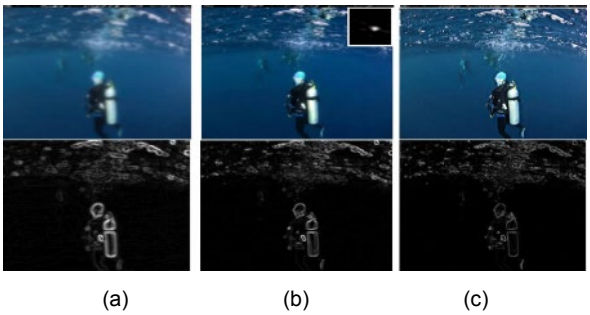

Fig. 11 Observed images (a), images enhanced and blur kernel estimated by Pan et al. (2016)'s method (b), and images enhanced by the proposed method (c)

4.2 Objective performance comparison

In quantitative analysis, two well-known no-reference image quality evaluation metrics (Yang and Sowmya, 2015; Panetta et al., 2016) have been applied, namely "underwater color image quality evaluation" (UCIQE) and "underwater image quality measure" (UIQM). UCIQE uses the standard deviation of chroma, the contrast of luminance, and the average saturation to represent the subjective quality perception. UIQM, inspired by the human visual system (HVS), uses the degradation model and imaging characteristics of underwater images. Simultaneously, underwater image colorfulness measure (UICM), underwater image sharpness measure (UISM), and underwater image contrast measure (UIConM) are used to evaluate the underwater image quality. Both metrics are proportional to the quality of images. The visual results of the restoring underwater images with the algorithms of Chiang and Chen (2012), Zhang et al. (2012), Galdran et al. (2015), and the proposed method are shown in Fig. 12. Zhang et al. (2012)'s method can improve the contrast to a certain extent, but it brings about color deviation. The proposed method provides better enhancement results than Galdran et al. (2015)'s method.

As shown in Figs. 13 and 14 and Tables 2 and 3, our method obtains the best results in terms of UCIQE and UIQM metrics.

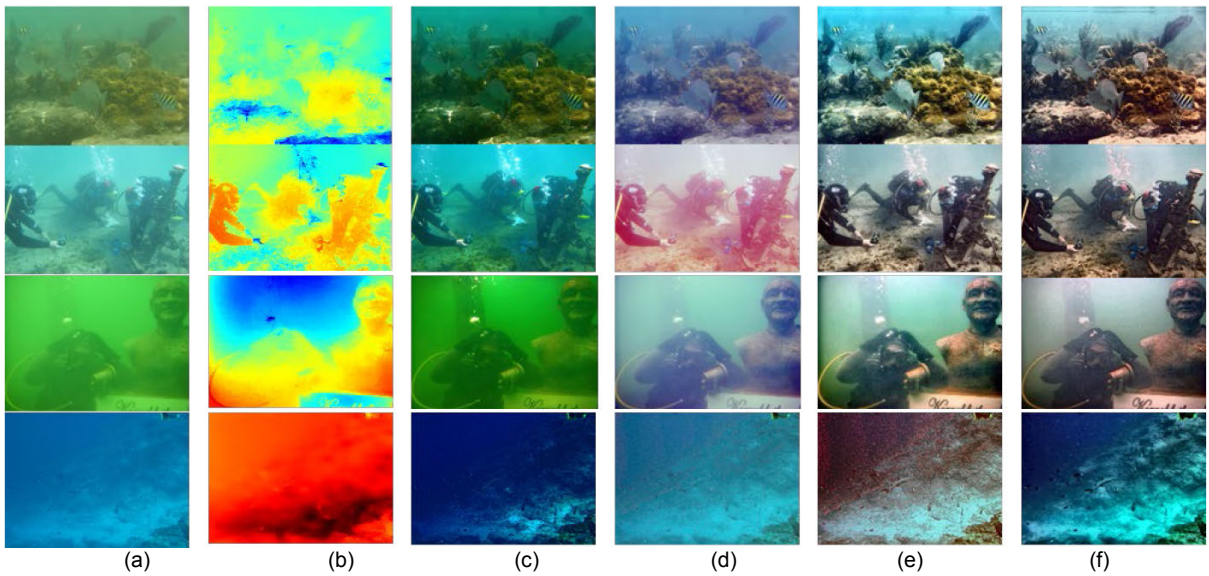

Fig. 12 Original images (a), transmission maps estimated by the proposed method (b), images enhanced by Chiang and Chen (2012)'s method (c), images enhanced by Zhang et al. (2012)'s method (d), images restored by Galdran et al. (2015)'s method (e), and images restored by the proposed method (f)

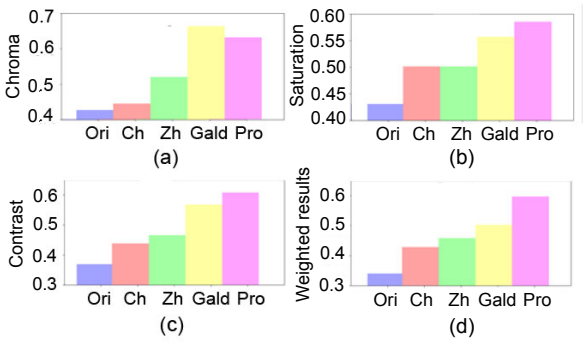

Fig. 13 Performance comparison in terms of UCIQE: (a) performance comparison of chroma; (b) performance comparison of saturation; (c) performance comparison of contrast; (d) performance comparison of weighted results

Ori: original method; Ch: Chiang and Chen (2012)'s method; Zh: Zhang et al. (2012)'s method; Gald: Galdran et al. (2015)'s method; Pro: the proposed method

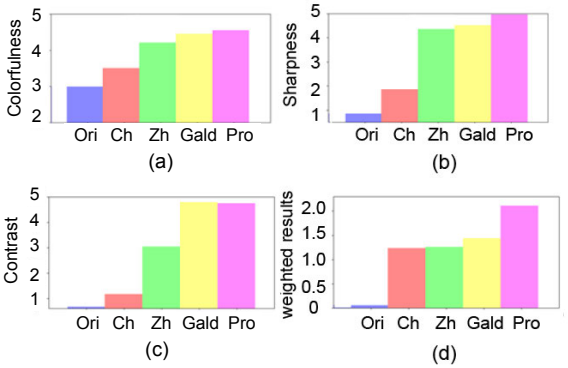

Fig. 14 Performance comparison in terms of UIQM: (a) performance comparison of colorfulness; (b) performance comparison of sharpness; (c) performance comparison of contrast; (d) performance comparison of weighted results

Ori: original method; Ch: Chiang and Chen (2012)'s method; Zh: Zhang et al. (2012)'s method; Gald: Galdran et al. (2015)'s method; Pro: the proposed method

Table 2 Performance comparison in terms of UCIQE

Image	Method				
	Ori	Ch	Zh	Gald	Pro
1	0.4269	0.4455	0.5209	**0.6638**	0.6321
2	0.4308	0.5016	0.5018	0.5573	**0.5857**
3	0.3693	0.4377	0.4650	0.5666	**0.6071**
4	0.2770	0.4282	0.4577	0.5030	**0.5972**

Ori: original; Ch: Chiang and Chen (2012)'s; Zh: Zhang et al. (2012)'s; Gald: Galdran et al. (2015)'s; Pro: proposed

Table 3 Performance comparison in terms of UIQM

Image	Method				
	Ori	Ch	Zh	Gald	Pro
1	2.9933	3.5056	4.2101	4.4518	**4.5439**
2	0.8634	1.8710	4.3513	4.5146	**4.9624**
3	0.6754	1.1648	3.0361	**4.7980**	4.7381
4	0.0664	1.2407	1.2719	1.4450	**2.1141**

Ori: original; Ch: Chiang and Chen (2012)'s; Zh: Zhang et al. (2012)'s; Gald: Galdran et al. (2015)'s; Pro: proposed

4.3 Applications

Additionally, we find that our method is suitable for several other applications described in this subsection.

Image segmentation aims to divide images into disjoint and homogeneous regions with respect to some characteristics (e.g., texture and color). Given the above-mentioned degradation of underwater images, there are defects in the segmentation results of underwater images. Fig. 15 demonstrates that our method can improve the segmentation performance.

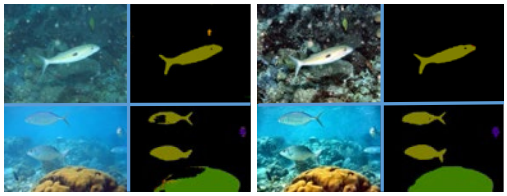

(a) (b) (c) (d)

Fig. 15 Image segmentation results: (a) raw underwater images; (b) raw underwater images' segmentation results; (c) restored images; (d) restored images' segmentation results

Note that our method can be directly applied to another kind of degraded images. Fig. 16 shows the experimental results of dust storm image de-hazing.

Test results demonstrate that the proposed method is actually a general framework for image preprocessing tasks.

Fig. 16 Results of dust storm image de-hazing

5 Conclusions

The problems of underwater images are those of detail loss and color distortion, because of backscattering and light attenuation. We have presented an end-to-end deep learning framework for transmission map estimation and single-image de-scattering. Since we cannot obtain the ground truth of clean images and corresponding hazy images, we have synthesized clean/hazy image pairs for convolutional neural network training. In the edge enhancement stage, we have transformed underwater images into the NSCT domain to remove noise and for edge enhancement. NSCT extracts more direction information of edges and produces better results than the traditional wavelet transform. Results have showed that the proposed method noticeably outperforms state-of-the-art methods in terms of subjective and objective performances. As shown in Section 4.3, our approach is suitable for atmospheric images and can be a general framework for image preprocessing tasks.

Acknowledgements

We would like to thank Miao YANG of the Department of Electronic and Engineering, Huaihai Institute of Technology, for providing the source code of the UCIQE metric.

Compliance with ethics guidelines

Pan-wang PAN, Fei YUAN, and En CHENG declare that they have no conflict of interest.

References

Ancuti C, Ancuti CO, Haber T, et al., 2012. Enhancing underwater images and videos by fusion. IEEE Conf on Computer Vision and Pattern Recognition, p.81-88. https://doi.org/10.1109/CVPR.2012.6247661

Cai BL, Xu XM, Jia K, et al., 2016. DehazeNet: an end-to-end system for single image haze removal. *IEEE Trans Image Process*, 25(11):5187-5198. https://doi.org/10.1109/TIP.2016.2598681

Carlevaris-Bianco N, Mohan A, Eustice RM, 2010. Initial results in underwater single image dehazing. OCEANS MTS/IEEE SEATTLE, p.1-8. https://doi.org/10.1109/OCEANS.2010.5664428

Chiang JY, Chen YC, 2012. Underwater image enhancement by wavelength compensation and dehazing. *IEEE Trans Image Process*, 21(4):1756-1769. https://doi.org/10.1109/TIP.2011.2179666

Drews P Jr, do Nascimento E, Moraes F, et al., 2013. Transmission estimation in underwater single images. IEEE Int Conf on Computer Vision Workshops, p.825-830. https://doi.org/10.1109/ICCVW.2013.113

Finlayson GD, Trezzi E, 2004. Shades of gray and colour constancy. The 12th Color Imaging Conf: Color Science and Engineering Systems, Technologies, Applications, p.37-41.

Galdran A, Pardo D, Picón A, et al., 2015. Automatic red-channel underwater image restoration. *J Vis Commun*

Image Represent, 26:132-145. https://doi.org/10.1016/j.jvcir.2014.11.006

Goodfellow IJ, Warde-Farley D, Mirza M, et al., 2013. Maxout networks. https://arxiv.org/abs/1302.4389?context=stat

He KM, Sun J, Tang XO, 2011. Single image haze removal using dark channel prior. *IEEE Trans Patt Anal Mach Intell*, 33(2):2341-2353. https://doi.org/10.1109/TPAMI.2010.168

Iqbal K, Odetayo M, James A, et al., 2010. Enhancing the low quality images using unsupervised colour correction method. IEEE Int Conf on Systems, Man and Cybernetics, p.1703-1709. https://doi.org/10.1109/ICSMC.2010.5642311

Li Y, Hu J, Jia Y, 2014. Automatic SAR image enhancement based on nonsubsampled contourlet transform and memetic algorithm. *Neurocomputing*, 134:70-78. https://doi.org/10.1016/j.neucom.2013.03.068

Mao BQ, Jin XM, 2010. Application of self-adaptive histogram equalization algorithm to image enhancement processing. *J Hebei North Univ (Nat Sci Ed)*, 26(5):64-68 (in Chinese). https://doi.org/10.3969/j.issn.1673-1492.2010.05.015

Padmavathi G, Subashini P, Kumar MM, 2010. Comparison of filters used for underwater image pre-processing. *Int J Comput Sci Netw Secur*, 10(1):58-65.

Pan JS, Sun DQ, Pfister H, et al., 2016. Blind image deblurring using dark channel prior. IEEE Conf on Computer Vision and Pattern Recognition, p.1628-1636. https://doi.org/10.1109/CVPR.2016.180

Panetta K, Gao C, Agaian S, 2016. Human-visual-system-inspired underwater image quality measures. *IEEE J Ocean Eng*, 41(3):541-551. https://doi.org/10.1109/JOE.2015.2469915

Schechner YY, Karpel N, 2006. Recovery of underwater visibility and structure by polarization analysis. *IEEE J Ocean Eng*, 30(3):570-587. https://doi.org/10.1109/JOE.2005.850871

Tan CS, Sluzek A, Seet GLG, et al., 2007. Range gated imaging system for underwater robotic vehicle. OCEANS Asia Pacific, p.1-6. https://doi.org/10.1109/OCEANSAP.2006.4393938

Tang KT, Yang JC, Wang J, 2014. Investigating haze-relevant features in a learning framework for image dehazing. IEEE Conf on Computer Vision and Pattern Recognition, p.2995-3002. https://doi.org/10.1109/CVPR.2014.383

Tarel JP, Hautiere N, Caraffa L, et al., 2012. Vision enhancement in homogeneous and heterogeneous fog. *IEEE Intell Trans Syst Mag*, 4(2):6-20. https://doi.org/10.1109/MITS.2012.2189969

Thakur VS, Tripathi N, 2010. On the way towards efficient enhancement of multi-channel underwater images. *Int J Appl Eng Res*, 5(5):895-903.

Tomasi C, Manduchi R, 1998. Bilateral filtering for gray and color images. Proc 6th Int Conf on Computer Vision, p.839-846.

Treibitz T, Schechner YY, 2009. Active polarization descattering. *IEEE Trans Patt Anal Mach Intell*, 31(3):385-399. https://doi.org/10.1109/TPAMI.2008.85

Vasamsetti S, Mittal N, Neelapu BC, et al., 2017. Wavelet based perspective on variational enhancement technique for underwater imagery. *Ocean Eng*, 141:88-100. https://doi.org/10.1016/j.oceaneng.2017.06.012

Wang HL, Cai WY, Yang JY, et al., 2015. Design of HD video surveillance system for deep-Sea biological exploration. Proc IEEE 16th Int Conf on Communication Technology, p.908-911. https://doi.org/10.1109/ICCT.2015.7399971

Yang AP, Zhang LY, Qu C, et al., 2017. Underwater images visibility improving algorithm with weighted L1 regularization. *J Electron Inform Technol*, 39(3):626-633 (in Chinese). https://doi.org/10.11999/JEIT160481

Yang M, Sowmya A, 2015. An underwater color image quality evaluation metric. *IEEE Trans Imag Proc*, 24(12):6062-6071. https://doi.org/10.1109/TIP.2015.2491020

Zhang SP, Zeng P, Luo XM, et al., 2012. Multi-scale retinex with color restoration and detail compensation. *J Xi'an Jiaotong Univ*, 46(4):32-37 (in Chinese).